Hydrol. Earth Syst. Sci. Discuss., https://doi.org/10.5194/hess-2018-616
Manuscript under review for journal Hydrol. Earth Syst. Sci.
Discussion started: 21 December 2018

Hydrology and Earth System Sciences
Open Access
Discussions

Modeling experiments on seasonal lake ice mass and energy balance in Qinghai-Tibet Plateau: A case study

Wenfeng Huang[1,2], Bin Cheng[3], Jinrong Zhang[1,2], Zheng Zhang[1,2], Timo Vihma[3], Zhijun Li[4,5], Fujun Niu[5]

[1] Key Laboratory of Subsurface Hydrology and Ecological Effects in Arid Region (the Ministry of Education), Chang'an University, Xi'an 710054, China

[2] School of Environmental Science and Engineering, Chang'an University, Xi'an 710054, China

[3] Finnish Meteorological Institute, Helsinki, Finland

[4] State Key Laboratory of Coastal and Offshore Engineering, Dalian University of Technology, Dalian 116024, China

[5] State Key Laboratory of Frozen Soil Engineering, Northwest Institute of Eco-Environment and Resources, Chinses Academy of Sciences, Lanzhou 730000, China

Correspondence to: Wenfeng Huang (huangwenfeng@chd.edu.cn)

Abstract. The lake-rich Qinghai-Tibet Plateau (QTP) has significant impacts on regional and global water cycles and monsoon systems through heat and water vapor exchange. The lake-atmosphere interactions have been quantified over open-water periods, yet little is known about the lake ice thermodynamics and heat and mass balance during ice-covered season due to a lack of field data. Modeling experiments on ice evolution and energy balance were performed in a shallow lake with a high-resolution snow and ice thermodynamic model. The bottom ice growth and decay dominated the seasonal evolution of the thickness of lake ice. Strong surface sublimation was a crucial pattern of ice loss, which was up to 40% of the maximum ice thickness. Simulation results matched well with the observations with respect to ice mass balance components, net ice thickness, and ice temperature. Strong solar radiation, consistent freezing air temperature, and low air moisture were the major driving forces controlling the seasonal ice mass balance. Energy balance was estimated at the ice surface and bottom, and within the ice interior and under-ice water. Particularly, almost all heat fluxes showed significant diurnal variations including short- and long-wave radiation, turbulent heat fluxes, water heat fluxes at ice bottom, and absorbed and penetrated solar radiation. The calculated ice surface temperature indicated that the atmospheric boundary layer was consistently stable and neutral over the ice-covered period. The turbulent heat fluxes between the lake ice and air and the net heat gain by the lake were much lower than those during open-water period. Ice surface sublimation (vapor flux) was demonstrated to be a vital seasonal water balance component, accounting for 41% of lake water loss during the ice seasons.

1. Introduction

The Qinghai-Tibet Plateau (QTP), characterized by a mean altitude of more than 4000 m above sea level (*asl*) and predominated by a freezing climate, is often referred to as the "Third Pole of the Earth". It harbors thousands of lakes covering a total area of approximately 40,700 km^2 and occupying approximately 50% of lakes located in China (Zhang et al., 2014). The QTP is also a headwater region of major Asian rivers including Yangtze, Yellow, Yarlung Tsangpo (Brahmaputra), Mekong, Salween, and Indus Rivers (Immerzeel et al., 2010). Due to its unique climatic environment (e.g. low air pressure and humidity, intense solar radiation, prevailing strong winds, widespread permafrost and glaciers, and dense lake/river network), QTP directly affects the regional and global water cycle, monsoon system, and atmospheric circulations (Wu et al., 2015; Li et al., 2016b; Su et al., 2016).

The lakes and ponds in QTP play an crucial role in the surface and subsurface hydrological processes (Pan et al., 2014), moisture and heat budgets (Wang et al., 2015; Li et al., 2016a, c; Wen et al., 2016), regional precipitation (Wen et al., 2015), engineering construction (Niu et al., 2011), and gas emission (Wu et al., 2014). They present dynamic variations on the annual base in terms of numbers and total area. The variations of size are probably due to warming and degradation of permafrost affected by the climate warming through, e.g. thermokarst (Niu et al., 2011), glacier retreating (Liao et al., 2013), increase of precipitation (Lei et al., 2013; Zhang et al., 2014) and strong surface evaporation. Turbulent heat and vapor vapour fluxes at the lake-air interface are crucial driving forces characterizing the lake-air interaction in numerical weather prediction (NWP) and climate models (Yang et al., 2015).

Despite the harsh climatic conditions and the difficulties in access to these lakes, some field campaigns have been performed during ice-free periods in recent years using eddy-covariance observations. An unstable or near-neutral atmospheric boundary layer (ABL) prevails over the QTP lake surface in summer (Wang et al., 2015; Li et al., 2015, 2016c). The turbulent heat fluxes show a strong seasonal variation and lag by 2–3 months behind net solar radiation (Li et al., 2016a; Wen et al., 2016). Heat flux dynamics over lake surface differ remarkably from those over other land surface types (like dry/wet grassland) (Biermann et al., 2014), emphasizing the need for a specific parameterization of lakes in surface schemes of NWP and climate models. However, the thermal regimes of lakes in QTP and their impacts on the atmosphere boundary layer and surrounding permafrost during wintertime (ice-covered season) remain unclear. Numerical models and parameterizations can be validated using observational data and will give deep insight into the lake-air interaction and lake thermal regime based on remote sensing datasets of meteorological variables and surface temperature (Kirillin et al., 2017; Wang et al., 2015; Wen et al., 2015).

Generally, the QTP lakes and ponds are ice-covered for 3–7 months, depending on their surface area, altitude, and regional climate (Kropáček et al., 2013). Lake ice thermodynamics (ice thickness and temperature) and phenology (the time of freeze-up and break-up, and the duration of the ice cover) play an important role in lake-air interaction (Li et al., 2016a), lake-effect snowfall (Wright et al., 2013), wintertime lake water quality and ecosystems (Kirillin et al., 2012), gas effluxes (Wu et al., 2014), and on-ice transport and operation. All of these issues highlight the accurate representation of QTP lake ice processes. Nevertheless, a few investigations on QTP lake ice have been conducted using field measurements and model simulations. Huang et al. (2012, 2013, 2016) reported the ice processes, interior structure, and thermal property in a small shallow thermokarst lake based on their *in situ* observations of years and provided significant insights into lake ice thermodynamics and its role in local heat and vapor fluxes and lake water budget. High-resolution remote sensing techniques and products were deployed tentatively to retrieve the QTP lake ice processes and provide a promising and convenient tool for lake ice research (Kropáček et al., 2013; Tian et al., 2015).

Thermodynamic modeling is an effective and robust methodology to understand lake ice processes and their relationship with local meteorological and hydrological conditions in polar, boreal and temperate regions (Cheng et al., 2014; Semmler et al., 2012; Yang et al., 2012).

In this study, we perform a modeling case study of a shallow lake located in the central QTP. Our objectives are (1) to identify major driving force that control the seasonal ice mass balance in QTP thermokarst lakes; (2) to quantify the components of mass and energy balance from the ice surface to bottom; (3) to estimate the lake-atmosphere heat and vapor fluxes through the whole ice-covered period. To the best of our knowledge, lake ice thermodynamic modeling in QTP has not been carried out before. We expect our work can provide a basis for further in situ measurements and upscaling of lake ice simulations over the QTP.

2. Methodology

2.1 Site description

The Beiluhe Basin is located in high pluvial and alluvial plain of the central QTP, with an elevation of 4500–4600 m *asl* (Fig. 1). The topography is undulating, covered by sparse vegetation and sand dunes. This basin is underlain by continuous permafrost 50-80m thick with the volumetric ice content of 30%–50% (Lin et al., 2017). During years 2004-2014, the mean annual air and ground temperatures varied from -2.9 ℃ to -4.1 ℃ and from -1.8 ℃ to -0.5 ℃, respectively (Lin et al., 2017). The annual mean precipitation ranged from 229 to 467 mm (average: 353 mm), while the annual mean potential evaporation ranged from 1588 to 1626 mm (average: 1613 mm) (Lin et al., 2017). There are more than 1200 lakes and ponds with the surface area larger than 1000 m^2 in the Beiluhe Basin. The largest lake has a surface area more than 60,000 m^2, and the average is 8500 m^2 (Luo et al., 2015). Lake depths are typically 0.5–2.5 m and the shapes are elliptical or elongated. About 20% of these lakes freeze to the bottom during winter (Lin et al., 2017).

Lake BLH-A (unofficial name) is located at 34°49.5′N, 92°55.4′E in Beiluhe Basin. The lake is perennially closed without rivers or streams flowing into and out of it. The minimum and maximum horizontal dimensions of the lake are 120 m and 150 m, respectively, making a total surface area of about 15,000 m^2. The maximum depth is 2.5 m with a stable water level through the year. The water is fresh and has a total dissolved solid of 1.30 g L^{-1}. Submerged plants grow abundantly in the lake sediment throughout the year. The lake has been investigated using in situ instrumentation and numerical modeling with respect to lake ice physics (Huang et al., 2011, 2016), hydrothermal regime (Lin et al., 2011), bank retrogression (Niu et al., 2011), and its disturbance to surrounding frozen ground (Lin et al., 2017). Considering physical properties of lake ice, a large number of gas bubbles have been found from the top layer of the ice cover. The large gas content caused a small bulk ice density (880–910 kg m^{-3}) and a small thermal conductivity (1.60–2.10 W m^{-1} K^{-1})) (Huang et al., 2012, 2013; Shi et al., 2014).

2.2 Field observations

Field campaigns were conducted in Lake BLH-A through three consecutive winters from 2010/2011 to 2012/2013, to record the ice-water-sediment temperatures, air temperature, and surface and bottom growth and decay of the ice cover. All equipments were mounted on a floater moored to the lake bank by four ropes. The floater was placed on the lake surface before the fall freeze-up, thus, all measures were recorded every 30 min through the whole ice season. The data yielded the following information: the dates of freeze-up and break-up (D_f and D_b) and time series of the vertical positions of (a) the ice-water interface (H_b), representing the basal melt or growth, and (b) the air-ice interface (H_s), representing the surface sublimation or/and melting. Hence, the evolution of ice thickness ($H = H_b – H_s$) was detected. For detailed information on instrumentation, see Huang et al. (2016).

The Beiluhe weather station (BWS), located 800 m southeast from the lake, monitored the air temperature (T_a), air relative humidity (*Rh*), atmospheric pressure (P_a), water vapor pressure in the air (e_a), wind speed (V_a) and direction, incident short- and long-wave irradiance (Q_l and Q_s) at 2 m and 10 m above the ground surface, and accumulated precipitation (water equivalent, *Prec*). In this paper we focus on the ice season of 2010/2011, when the observed datasets have the highest quality and least missing values. Furthermore, the data reveal a typical seasonal cycle of the lake ice phenology (Fig. 2).

In early freezing season in late October, a thin ice layer typically formed at nights and melted during daytime. Finally, a stable ice cover formed in early November (freeze-up). A strong surface sublimation process at the ice-air interface was observed through the whole ice season, reducing the total ice thickness congealed from the ice-water interface. The absolute thickness reached its maximum (~ 60 cm) in early February. On the basis of our field visits during freezing (early December) and melting (late March) stages and the constant low temperature and strong wind through the ice season, we concluded that the ice surface was most probably persistently dry throughout the 2010/2011 ice season.

2.3 Thermodynamic snow and ice model

A well calibrated (Launiainen and Cheng, 1998, Vihma et al., 2002) and widely used (Cheng et al., 2006, 2008; Semmler et al., 2012; Yang et al., 2012; Cheng et al., 2014) thermodynamic snow and ice model (HIGHTSI) is applied in this study to investigate Lake BLH surface energy and ice mass balances. The surface heat balance reads:

$$(1-\alpha)(1-\gamma)Q_s + \varepsilon\sigma T_s^4 + Q_{le} + Q_h + Q_p + F_c = F_m \qquad (1)$$

where Q_s and Q_l is the incident shortwave and longwave radiation, respectively, α is the surface albedo, γ is the fraction of solar radiation penetrating the surface, ε is the thermal emissivity of the surface (ice/snow), σ is the Stefan-Boltzmann constant, T_s is the surface temperature, Q_{le} and Q_h are the latent and sensible heat fluxes, Q_p is the heat flux from precipitation, which can be neglected in QTP during wintertime, F_c is the conductive heat flux in the ice at the surface, and F_m is the surface heat balance. Surface melting is accordingly calculated as:

$$\rho_i L_f \frac{dH}{dt} + F_m = k_{iup}\frac{\partial T}{\partial z} \qquad (2)$$

where ρ_i is the ice density, L_f is the latent heat of freezing, k_{iup} is the thermal conductivity of ice at upper ice layer, T is the ice temperature, and z is the vertical coordinate. The incident short- and longwave radiative fluxes are either parameterized, taking into account cloudiness, or prescribed by observations or NWP model output. The penetration of solar radiation into the snow and ice is parameterized according to surface albedo and optical properties of snow and ice. The turbulent heat fluxes (Q_e and Q_c) at ice-air interface are parameterized using the bulk-aerodynamic formulae as follows:

$$Q_{le} = \rho_a L C_e V_a (q_s - q_a) \qquad (3)$$

$$Q_h = \rho_a c_p C_h V_a (T_s - T_a) \qquad (4)$$

where ρ_a is the air density, L is the latent heat of sublimation of ice when T_s < 0 ℃ or of evaporation of water when $T_s \geq 0$ ℃, V_a is the wind speed at the reference height (2.0 m), q_s and T_s are the specific humidity and air temperature at the ice surface, q_a and T_a are the specific humidity and temperature of air at the reference height, and C_e and C_h are the bulk transfer coefficients for heat and water vapor, respectively. Both transfer coefficients are parameterized taking into account the thermal stratification of the atmospheric boundary layer (Launiainen and Cheng, 1998; Wang et al., 2015). In addition, Q_{le}/L gives the equivalent thickness of sublimated ice or of evaporated water E.

$$E = \frac{Q_{le}}{L} \quad (5)$$

At the bottom boundary, the ice growth/melt is calculated on the basis of the difference between the heat flux from lake water to ice base (F_w) and the conductive heat flux at the ice bottom layer:

$$\rho_i L_f \frac{dH}{dt} + F_w = k_{idn} \frac{\partial T}{\partial z} \quad (6)$$

where k_{idn} is the thermal conductivity of ice at ice bottom layer. In HIGHTSI, F_w is either prescribed as a constant value or prescribed based on in situ observations.

The evolutions of thickness and temperature of snow and ice are obtained by solving the heat conduction equations for multiple ice and snow layers. Eq (1) solves the surface temperature, which is used as the upper boundary condition as well as to determine whether surface melting occurs. The ice bottom temperature keeps at the freezing point.

2.4 Meteorological data and model parameters

The meteorological data are based on the BWS (Fig. 3). The 2-m air temperature observed on the lake site was highly correlated with the measurement at BWS station (R^2 = 0.98). The T_a has a strong diurnal cycle in response to the large diurnal cycle of solar radiation. The mean T_a was -10.6 ℃ during simulation period from Day 313 (Nov. 9, 2010) to Day 480 (Apr. 25, 2011). The northwest winds prevailed during the winter season. The gust wind speed was frequently larger than 10 m/s. The average wind speed was 6.5 m s^{-1} associated with an average relative humidity of 34 % only.

The daily insolation lasted for 10-12 hours and the average daily solar radiation *Qs* was about 390 W m^{-2} during the simulation period, with the daily maximum ranging from 570 to 1140 W m^{-2}. The averaged downward longwave radiation during daytime (8:00-19:00) and nighttime (20:00-7:00) was approximately 177 and 180 W m^{-2}, respectively. The net longwave cooling was strong during nighttime.

The snow pack was very thin, literally zero, during winter 2010/2011. There were a few minor snowfall events, but no snow accumulation because of strong wind. A major detectable snowfall occurred in early April (~ 9 cm of snow), but the snow was blown off in a short time. For simplicity, snow was not taken into account in the model simulation. The transparent ice allowed solar radiation to penetrate into the ice interior and further down to the under-ice water column, heating the ice/water column daily.

The sky was persistently clear over the whole ice season 2010/2011. The high cloudiness and overcast condition occurred only during late ice season. A slight thin film of fine sand accumulated on the ice surface in early spring coloring the ice surface light yellow. The surface albedo may have accordingly reduced, leading more solar radiation absorption at and below the surface. An albedo parameterization scheme for a climate system model developed by Briegleb et al., (2004) was applied in this study, but the impact of the surface dust film was not taken into consideration.

When running the HIGHTSI model, we have to input values of the heat flux F_w. which is quite challenging to be observed. Actually, we estimate F_w using heat residual method at ice base based on *in situ* measurements of in-ice temperature profile and the rate of basal ice growth (Huang et al., to be submitted). But for a reference run, a prescribed time series for the derived F_w was used. The average F_w was approximated 27 W m^{-2}.

For the reference run, model forcing data and parameters were given in Table 1.

Hydrol. Earth Syst. Sci. Discuss., https://doi.org/10.5194/hess-2018-616
Manuscript under review for journal Hydrol. Earth Syst. Sci.
Discussion started: 21 December 2018

3. Results and analysis

3.1 Lake ice thickness and mass balance

The BLH-A lake ice congelation lasted from early November to the beginning of February. Through February, the ice growth reached a thermal equilibrium stage, and the ice thickness did not change much. From the beginning of March, the ice started to melt, most at the ice bottom and also within the ice interior. Finally, the ice cover disappeared at the end of April. The growth, thermal equilibrium, and melting periods lasted for approximately 87, 30, and 56 days, respectively.

The lake ice mass balance consists of several components (Fig. 4a). The ice bottom evolution (congelation ice) dominated the ice growth to 0.75 m until day 430 before a melting started at the ice bottom. The model calculated a total surface melting (~0.12 m) at the end of the ice season. A strong loss of latent heat flux during the entire period generated some 0.23 m of lake ice sublimation at the ice surface. The observed air-ice interface evolution (Fig. 2) revealed the integrated impacts of surface sublimation and melting (during the late season), which could not be instrumentally delineated from each other. By regrouping the modeled ice mass balance components, we can calculate the evolution of the ice surface (i.e. surface sublimation + melting) and ice bottom, and compare them with the measurements (Fig. 4b). Although the modeled bottom depth is 4.2 cm larger than measured one (Table 2), the HIGHTSI model very well captured the general evolution both at the ice surface and bottom. The modeled total ice thickness (i.e. $Depth_B$–$Depth_S$) is in good agreement with the observations (Fig. 4c). However, during day 460, the ice melting was stopped due to a snowfall event. This short-term pause was not revealed by the model since the snow thickness was assumed zero.

HIGHTSI modeling also affirmed that there are obvious and strong diurnal cycles of freezing and melting at the ice bottom when the ice thickness is less than ~ 20 cm, especially in late spring. For instance, during the melting stage, the ice melts rapidly from 9:00-10:00 to 17:00-18:00, and undergoes an equilibrium or minor growth from 18:00 to 6:00-8:00, then melts again during daytime at the bottom. Besides, the model also detected diurnal variations in the surface sublimation and melting.

Statistical analysis indicated that the model results and measurements for ice mass balance have a high correlation ($R > 0.97$) and small standard deviations (< 3.6 cm), and match very well in terms of surface and bottom depth evolutions and ice thickness with *MAEs* and *RMSEs* generally lower than 5.5 cm (Table 2).

3.2 Lake ice temperatures

The modeled ice temperature regime (Fig. 5) revealed that there are strong diurnal cycles in ice temperature throughout the ice season, following the large diurnal cycle in air temperature and solar radiation. This is consistent with the observed ice thermal dynamics. The calculated surface temperature of ice was continuously lower than the freezing point, except during daytime in late April, when it reveal at the melting point causing some cycles of daytime-melting and nighttime-freezing at the surface.

The calculated and observed vertical profiles of ice temperature were compared at selected time steps (Fig. 6). The ice temperature was modeled quite well during the ice growth period (Figs. 6a-d). During the equilibrium and melting stages, the observed and modeled temperature discrepancies were larger especially at the surface and bottom parts. This could have resulted from several processes. From the beginning of the equilibrium stage, the solar radiation increased gradually and was absorbed by the thermistor sensors at top layer, leading to higher observed values near the surface during daytime (Fig. 6e). During the melting period, the bottommost part of the ice column underwent fast phase change, and the inter-crystal spaces could be filled with underlying warm water. The sensors near the ice bottom actually detected the integrated temperature of ice and water, thus the observed temperature could be quite close to and even slightly higher than the freezing point (0 ℃) (Figs. 6e,f). On the other hand, the linearly interpolated surface depth is likely to cause errors in determining the true sensor depths within the sublimating ice cover, causing some temperature differences.

3.3 Modeled Energy balance

The lake ice thickening and thinning and temperature regime (i.e. phase transitions) are governed by the energy transport and translation through the air-ice-water column. The good performances of HIGHTSI model in calculating the ice mass balance and temperature dynamics argue comprehensive estimates of heat/radiation transfer and partitioning within the air-ice-water column. For a seasonal cycle, the monthly means of various heat fluxes were calculated at the ice surface, within the ice interior, and at the ice bottom (Table 3).

The net shortwave radiation (Q_{sn}) absorbed by the lake acted as a main energy source for ice and water thermodynamics, and followed the seasonal variation of total incident solar radiation (Q_s). The Q_{sn} penetrated through the ice surface and interior, and into the under-ice water column, thus, it was divided into three parts: the net solar radiation used for surface energy balance ($Q_{ss}=(1-\alpha)(1-\gamma)Q_s$) (~43% of Q_{sn}), the absorption by the ice interior beneath surface (Q_{si}) (~36%), and the absorption by water (Q_{sw}) (~21%), all of which also showed similar seasonal variation to Q_s. The water heat flux into ice (F_w) represents the temperature difference between the water and ice bottom, was larger when the ice was thinner. The turbulent heat fluxes did not show strong seasonal variations through the ice season. Furthermore, almost all of the heat fluxes showed strong diurnal variations (Fig. 7). All radiative fluxes (Q_s, Q_{sn}, Q_{si}, and Q_{sw}) had synchronous diurnal cycles, peaked at noon and disappeared through night. The sensible heat flux (Q_h) peaked in the afternoon and had its minimum just before the dawn. The latent heat flux (Q_{le}) had an opposite diurnal pattern with a minimum in the afternoon and maximum in the early morning. The net longwave radiation (Q_{ln}) and surface conductive heat flux (F_c) had a roughly opposite diurnal phase to each other with extremes appeared in the midnight.

At the surface (i.e. the surface layer in the model), the upward conductive heat flux (F_c) represents the near surface ice temperature gradient. When the ice was thin (e.g. in November), the larger F_c indicates more heat lost from the ice bottom to surface, and thus rapid ice growth. The net long-wave radiation ($Q_{ln}=Q_l-\varepsilon\sigma T_s^4$) was consistently negative and indicated the cold ice surface emitted the heat back to the air/space all the time. The sensible heat flux (Q_h) was generally positive, thus argued heat gain from the air. The large negative latent heat flux (Q_{le}) (Table 3) manifested the surface sublimation was strong (Fig. 4a). For the surface heat balancing (Eq. 1), the residual F_m was close to zero, indicating a dry cold surface. But in April, its positive value revealed the ice melted at surface (Fig. 4a), and the latent heat was induced by the evaporation of meltwater during late melting season instead of the sublimation of ice.

Within the ice interior, the absorbed solar radiation Q_{si} was used to heat the ice during daytime and thus caused the diurnal variation in ice temperature (Fig. 5), and also led to internal melting in way of gas pore expansion during the late ice season (Leppäranta et al., 2010).

Beneath the ice bottom, the under-ice water column absorbed the transmitted solar radiation Q_{sw} and raised its temperature at daytime. According to the lake sediment temperature measurements in BLH-A by Lin et al. (2011, 2017), through the whole ice-covered season the bottom sediment releases quite limited heat to lake water (– 0.2~ –0.6 W m^{-2}), consequently, this heat flux can be ignored. For the energy balance of under-ice water, the penetrated solar radiation is the pivotal heat source, of which 56% is released into the ice bottom (F_w), 44% is used to increase the bulk water temperature and partly is transformed to turbulent kinetic energy forcing water convection, and few (< 0.1%) is transported to bottom sediment (permafrost and talik).

3.4 Model experiment on F_w

Usually, F_w is assumed to be constant throughout an ice season when simulating ice thickness in Arctic or temperate lakes. Therefore, under the same weather forcing condition, a number of model experiments have been carrying out using constant F_w (0–50 W m^{-2} with an interval of 5 W m^{-2}).

During modeling period, the average ice growth at bottom was 0.49 m with a maximum ice growth of about 0.72 m. The average and maximum ice thicknesses were 0.38 m and 0.61 m, respectively. Model experiments indicated that the average F_w cannot be smaller than 15 W m^{-2} because otherwise both average and maximum ice thicknesses differ a lot from observations (Fig. 8). If average F_w is about 35 W m^{-2}, the modeled average and maximum net total ice thickness are not far from the observed values, but have large offsets at ice bottom, especially for the maximum ice growth at ice bottom. If average F_w is more than 35 W m^{-2}, the errors for both average and maximum ice thicknesses are getting larger. It seems when average F_w is between 20 W m^{-2} and 30 W m^{-2}, the modeled results are within the ranges of observed values with respect to total and bottom growth ice thicknesses.

In reality, F_w is not a constant value. Model experiments argued that the mass balance at ice base cannot be reproduced using constant F_w through the whole ice season. Based on heat residual method, we created the time series of F_w (Fig. 9) to carry out the reference run (Fig. 4) that gave a very good agreement to the observations.

Differ from the ocean and large deep lake, where the variation of F_w is largely driven by the under-ice currents (Krishfield and Perovich, 2005; Rizk et al., 2014), BLH-A was very shallow and the water below ice is largely at a standstill, so the driving force for F_w most likely is the penetrated solar radiation. The modeled solar radiative flux that penetrates through the ice layer and reaches at ice bottom is plotted in Fig. 9. In early simulation, ice was very thin and surface albedo is small, so large part of solar radiation penetrated through ice layer and warmed the underlying water, creating large F_w. When ice was getting thicker, surface albedo increased and penetrated solar radiation was reduced. In later part of the season, melting of ice reduced surface albedo, the downward solar radiation from sky was increased, and thus, more solar radiation was accordingly absorbed in the lake water below ice. The average solar radiation absorbed by under-ice water column during entire simulation period was 22 W m^{-2}. Additionally, the specific heat flux from underlying water temperature change was estimated of 3 W m^{-2}. The total 25 W m^{-2} is in the range of good agreement between observed and modeled ice thickness (Fig. 8).

4. Discussion

4.1 Implication on ABL over ice-covered lakes

The characteristics of the ABL play a direct role in the turbulent heat and mass fluxes and thus the effects of lakes on local and regional monsoon systems and water cycles. Recent findings indicated that the air-lake energy exchange in QTP is characterized by a persistent unstable air-lake boundary layer through the open-water period (Li et al., 2015; Wang et al., 2015; Wen et al., 2016). The modeled and observed temperature profiles of air-ice-water column presented here can give a close insight into the air-lake boundary layer features during the ice-covered period taking the temperature difference between the lake (ice) surface and the air as a bulk stability indicator. The ice surface temperature (T_s) was generally lower than the air temperature (T_a). The monthly mean T_s was consistently lower than the monthly T_a by 1.24 ± 0.55 °C from December through April, indicating a persistent stable atmposphere boundary layer through the ice-covered period (Fig. 10). However, the T_s was 0.31 °C higher than T_a in November when the ice was rapidly growing, especially when the ice thickness was less than ~ 10 cm (i.e., before Nov. 20).

Previous investigations revealed that the QTP lakes are predominantly characterized by unstable ABL during open-water period (Li et al., 2015; Wang et al., 2015; Wen et al., 2016). The present results indicated that the air-lake boundary layer turns into a stable or neutral stratification soon after the lake ice forms. When the lake ice disappears, the air boundary layer soon turns into an unstable straitfication again (Wen et al., 2016). However, short-term periods of unstable boundary conditions were observed for approximately 25% of the ice duration period. The unstable conditions usually took up on diurnal scale especially following sudden drops of the air temperature.

4.2 The air-lake heat exchange

Diurnal changes in turbulent heat fluxes, however, are large which were commonly seen for high latitude and high altitude lakes (e.g. Vesala et al., 2006; Rouse et al., 2008; Nordbo et al., 2011; Wang et al. 2015; Li et al. 2016a, c; Wen et al. 2016). In our study, the mean values of turbulent heat fluxes of Q_h and Q_{le} are 14.1 W m^{-2} and –41.3 W m^{-2}, respectively. These numbers are in line with observations that were obtained in QTP lakes in winter season (Li et al., 2016a). For an intra-annual comparison, the Q_h and Q_{le} over lake ice are approximately 40%–60% lower compared with those over open-water lake, indicating the ice-covered lakes have different heat flux dynamics to the open-water ones. The present turbulent heat fluxes are somehow greater than those observed at Great Slave Lake and a boreal lake in south Finland during open-water period (Blanken et al., 2000; Nordbo et al., 2011). This is attributed to the larger wind speed and drier air prevailing over the QTP.

The net heat exchange ($Q_{net}= Q_{sn} +Q_{ln}+Q_h+Q_{le}$) through the atmosphere-lake interface showed strong diurnal and seasonal cycle. Q_{net} increased gradually through the whole ice season. The lake ice released heat into the atmosphere before early March, and then absorbed heat from the atmosphere. Integrated over the ice season, the lake released heat of about 266 MJ m^{-2} (i.e. ~17 W m^{-2}).

4.3 Water vapor flux and lake water balance

The water balance in a lake reads

$$\Delta V = P - E + R_s + R_g \qquad (7)$$

where ΔV is the lake water change, and P, E, R_s and R_g are the precipitation, evaporation, net surface inflow and subsurface inflow, respectively.

During the freezing season in central QTP, the precipitation is generally quite small and the surface inflow and outflow through gullies and streams are typically blocked due to the freezing conditions. Therefore, the lake water balance is strongly affected by evaporation/sublimation and subsurface inflow/outflow.

Assuming ice density of 900 kg m^{-3}, the modeled sublimated ice thickness E can be converted to water equivalent (*WE*) (Fig. 12). The monthly mean sublimation was the weakest in December and January, but higher in February and March. This is probably due to the higher air temperature, stronger winds, and more incident long- and short-wave radiation than before according to Eqs (3) and (5) (Fig. 3). Through the entire ice season, the ice surface water loss due to evaporation/sublimation was approximately 207 mm *WE*.

The BLH-A lake water level observations revealed a decreasing of 0.50 m through the whole ice season (Lin et al., 2017). The surface evaporation/sublimation hence accounts for 41% of lake water loss during the ice-covered period. The remaining part of water loss is probably caused by vertical percolation through the lake sediment to supply deep groundwater, since the talik beneath the lake has developed through the underlying permafrost (Lin et al., 2011, 2017; Niu et al., 2011), and by the lateral water discharge into ambient soil during the thickening and thinning of frozen active layer (Pan et al., 2014; Lin et al., 2017).

5. Summary and conclusion

The ice season was characterized by a freezing period (9 November – 4 February), a thermal equilibrium period (5 February –10 March), and a melting period (11 March – 30 April). During the freezing period, strong atmospheric cooling caused a growth of congelation ice of about 70 cm. The major driving force for ice growth was a consistent subzero air temperature (mean -13 ℃) and a strong average net longwave radiative cooling (-97 W m^{-2}), although the ice surface absorbed a net downward solar radiative flux of 77 W m^{-2} on the average.

During melting period, the ice melt rate was about 14 mm/day. Basal melting dominated and surface melting was seen only by the very end of the ice season, because air temperatures remained subzero during most of the winter. A total 0.23 m of ice thickness was lost at the surface due to a sustained sublimation process during the entire study period. This is caused by a combined effect of prevailing strong winds and dry air. The observed average wind speed and relative humidity were 7 m s^{-1} and 34%, respectively.

Ice thickness modelled by HIGHTSI was in good agreement with observations, in particular the total ice thickness. The surface sublimation and basal freezing and melting as well as ice temperature regimes were comparable to those observed. The modelled surface energy balance indicated that the net long-wave radiative cooling (-97 W m^{-2}) and upward conductive heat flux in the ice interior as well as turbulent latent heat flux dominated the ice surface energy and mass balance. The average net solar radiative flux was large (181 W m^{-2}); 40% of it was reflected back to the space, 34% was absorbed below the ice surface, and only 26% was used for surface energy balance. Diurnal cycles of surface heat fluxes were driven by the diurnal variations of shortwave radiation. The observed air temperature and calculated ice surface temperature suggested a consistent stably stratificated ABL uring most of the ice-covered period, except when the ice thickness was less than ~10 cm. Through the whole ice-covered season, the lake (ice) released 17 W m^{-2} heat to the atmosphere.

The ice surface mass balance was dominated by surface ice sublimation, which was modeled very well. The sublimation was demonstrated to be a key component for lake water balance and accounted for 41% of lake water loss during wintertime. In light of the generally low air humidity and strong wind over QTP, the sublimation can be critical for the water balance of a large number of shallow lakes and ponds over the QTP, and further research (obs and mod) is needed for the quantification of sublimation in a regional scale over QTP.

The water-ice heat flux F_w controlled the basal, and thus, the net ice thickness evolution. The model experiments indicated that constant F_w through the whole ice season cannot produce a reasonable basal mass balance. A parameterized time series of F_w was used and gave realistic results. This confirmed the temporal variation in F_w in shallow QTP thermokarst lakes. Many more observing efforts should be made to quantify it and its governing physics.

The present modeling indicated that the largest uncertainty for QTP lake ice modeling is the effect of F_w. Thermokarst lakes on QTP are typically shallow and small, without significant surface water input and output, implying that through-lake current or lake-wide circulation under the ice cover are negligible (Kirillin et al., 2015). Cold sediment layer limits heat release into the overlying water (Lin et al., 2011). However, the solar radiation is strong (due to persistent clear sky condition), and the lake ice cover is consistently free of snow. In QTP, the surface albedo of ice in large lakes can be unprecedentedly small (Li et al., 2018). Indeed, in our study the Briegleb albedo scheme yielded small albedo, in particular, when the ice was thin. Intensive penetrative solar radiation can drive under-ice turbulent mass and heat mixing (Mironov et al., 2002), however, the quantitative effect of solar penetration on F_w is still not yet know, and needs new field experiments.

Snow is neglected in this modeling work, however, snowfall occasionally occur on QTP and it may have a strong impact in ice mass balance, especially for large lakes (Cheng et al., 2014). The major impact of snow on ice thermodynamics is the insulation effect (Leppäranta, 2015). Snow-ice is not likely to form on QTP, since in early winter the air temperature drops fast and the ice freezes quickly. However, superimposed ice may happen in late spring if there is thick snow on top of ice. Otherwise, snow can compensate the strong ice mass loss due to sublimation, cutting down water loss in QTP lakes in winters.

Data availability. The datasets on lake ice temperatures and thickness, and meteorology used for modeling and comparison can be downloaded from http://www.researchgate.net/profile/Wenfeng_Huang.

Competing interests. The authors declare no competing interests.

Acknowledgements. This work is supported by the National Natural Science Foundation of China (41402203, 51579028), the Natural Science Fund of Shaanxi Province (2018JQ4021), the Special Fund for Basic Scientific Research of Central Colleges (310829171002, 310829161006), and the Open Fund of State Key Laboratory of Frozen Soils Engineering (SKLFSE201604). We are also grateful to the staff from the Field Station of Permafrost Engineering and Environmental Tests for their field assistance, and PEEX program for providing international cooperation.

References

Biermann, T., Babel, W., Ma, W., Chen, X., Thiem, E., Ma. Y., and Foken, T.: Turbulent flux observations and modeling over a shallow lake and a wet grassland in the Nam Co basin, Tibetan Plateau, Theor. Appl. Climatol., 116, 301-316, 2014.

Blanken, P.D., Rouse, W.R., Culf, A.D., Spence, C., Boudreau, L.D., Jasper, J.N., Kochtubajda, B., Schertzer, W.M., Marsh, P., and Verseghy, D.: Eddy covariance measurements of evaporation from Great Slave Lake, Northwest Territories, Canada, Water Res. Res., 36(4), 1069-1077, 2000.

Briegleb, B., Bitz, C.M., Hunke, E.C., Lipscomb, W.H., Holland, M.M., Schramm, J., and Moritz, R.: Scientific description of the sea ice component in the Community Climate System Model, Ver. 3, NCAR/TN-463+STR, NCAR Tech Note, 1-78, 2004.

Cheng, B., Vihma, T., Rontu, L., Kontu, A.: Evolution of snow and ice temperature, thickness and energy balance in Lake Orajärvi, northern Finland, Tellus A, 66, 21564, http://dx.doi.org/10.3402/tellusa.v66.21564, 2014.

Cheng, B., Vihma, T., Pirazzini, R., and Granskog, M.: Modeling of superimposed ice formation during spring snowmelt period in the Baltic Sea, Ann. Glaciol., 44, 139–146, 2006.

Cheng, B., Zhang, Z., Vihma, T., Johansson, M., Bian, L., Li, Z., and Wu, H.: Model experiments on snow and ice thermodynamics in the Arctic Ocean with CHINARE 2003 data, J. Geophys. Res., 113, C09020, doi:10.1029/2007JC004654, 2008.

Huang, W., Han, H., Shi, L., Niu, F., Deng, Y., and Li, Z.: Effective thermal conductivity of thermokarst lake in Beiluhe Basin, Qinghai-Tibet Plateau, Cold Reg. Sci. Technol., 85, 34-41, 2013.

Huang, W., Li, R., Han, H., Niu, F., Wu, Q., and Wang, W.: Ice processes and surface ablation in a shallow thermokarst lake in the central Qinghai-Tibet Plateau, Ann. Glaciol., 57(71), 20-28, 2016.

Huang, W., Li, Z., Han, H., Niu, F., Lin, Z., and Leppäranta, M.: Structural analysis of thermokarst lake ice in Beiluhe Basin, Qinghai-Tibet Plateau, Cold Reg. Sci. Technol., 72, 33-42, 2012.

Immerzeel, W.W., van Beek, L.P.H., and Bierkens, M.F.P.: Climate change will affect the Asian water towers, Science, 328, 1382-1385, 2010.

Jonas, T., Terzhevik, A.Y., Mironov, D.V., and Wüest, A.: Radiatively driven convection in an ice-covered lake investigated by using temperature microstructure technique, J. Geophys. Res., 108(C6), 3183, doi: 10.1029/2002JC001316, 2003.

Kirillin, G.B., Forrest, A.L. Graves, K.E., Fischer, A., Engelhardt, C., and Laval, B.E.: Axisymmetric circulation driven by marginal heating in ice-covered lakes, Geophys. Res. Lett., 42, 2893-2900, 2015.

Kirillin, G., Leppäranta, M., Terzhevik, A., Granin, N., Bernhardt, J., Engelhardt, C., Efremova, T., Golosov, S., Palshin, N., Sherstyankin, P., Zdorovennova, G., and Zdorovennov, R.: Physics of seasonally ice-covered lakes: a review, Aquat. Sci., 74(4), 659-682, 2012.

Kirillin, G., Wen, L., and Shatwell, T.: Seasonal thermal regime and climatic trends in lakes of the Tibetan Highlands, Hydrol. Earth Syst. Sci., 21, 1895-1909, 2017.

Krishfield, R.A., and Perovich, D.K.: Spatial and temporal variability of oceanic heat flux to the Arctic ice pack, J. Geophys. Res., 110, C07021, doi: 10.1029/2004JC002293, 2005.

Kropáček, J., Maussion, F., Chen, F., Hoerz, S., and Hochschild, V.: Analysis of ice phenology of lakes on the Tibetan Plateau from MODIS data, The Cryosphere, 7, 287-301, 2013.

Launiainen, J., and Cheng, B.: Modeling of ice thermodynamics in natural water bodies, Cold Reg. Sci. Technol., 27(3), 13-178, 1998.

Lei, Y., Yao, T., Bird, B. W., Yang, K., Zhai, J., and Sheng, Y.: Coherent lake growth on the central Tibetan Plateau since the 1970s: Characterization and attribution, J. Hydrol., 483(3), 61-67, 2013.

Leppäranta, M.: Freezing of lakes and the evolution of their ice cover, Springer, Berlin,

Hydrol. Earth Syst. Sci. Discuss., https://doi.org/10.5194/hess-2018-616
Manuscript under review for journal Hydrol. Earth Syst. Sci.
Discussion started: 21 December 2018

Hydrology and Earth System Sciences
Open Access
Discussions

Heidelberg, 2015.

Leppäranta, M., Terzhevik, A., and Shirasawa, K.: Solar radiation and ice melting in Lake Vendyurskoe, Russian, Hydrol. Res., 41(1), 50-62, 2010.

Li, X., Ma, Y., Huang, Y., Hu, X., Wu, X., Wang, P., Li, G., Zhang, S., Wu, H., Jiang, Z., Cui, B., and Liu, L.: Evaporation and surface energy budget over the largest high-altitude saline lake on the Qinghai-Tibet Plateau, J. Geophys. Res.- Atmos., 121(18), 10470-10485, 2016a.

Li, Y., Zhang, C., and Wang, Y.: The verification of millennial-scale monsoon water vapor transport channel in northwest China, J. Hydrol., 536, 273-283, 2016b.

Li, Z., Ao, Y., Lyu, S., Lang, J., Wen, L., Stepanenko, V., Meng, X., and Zhao, L.: Investigations of the ice surface albedo in the Tibetan Plateau lakes based on the field observation and MODIS products, J. Glaciol., doi: 10.1017/jog.2018.35, 2018.

Li, Z., Lyu, S., Zhao, L., Wen, L., Ao, Y., and Wang, S.: Turbulent transfer coefficient and roughness length in a high-altitude lake, Tibetan Plateau, Theor. Appl. Climatol., 124, 723-735, 2016c.

Li, Z., Lyu, S., Ao, Y., Wen, L., Zhao, L., and Wang, S.: Long-term energy flux and radiation balance observations over Lake Ngoring, Tibetan Plateau, Atmos. Res., 155, 13-25, 2015.

Liao, J., Shen, G., and Li, Y.: Lake variations in response to climate change in the Tibetan Plateau in the past 40 years, Int. J. Digit. Earth, 6(6), 534-549, doi:10.1080/17538947.2012.656290, 2013.

Lin, Z.J., Niu, F.J., Fang, J.H., Luo, J., and Yin, G.A.: Interannual variations in the hydrothermal regime around a thermokarst lake in Beiluhe, Qinghai-Tibet Plateau, Geomorphology, 276, 16-26, 2017.

Lin, Z., Niu, F., Liu, H., and Lu, J.: Hydrothermal processes of alpine tundra lakes, Beiluhe Basin, Qinghai-Tibet Plateau, Cold Reg. Sci. Technol., 65, 446-455, 2011.

Luo, J., Niu, F., Lin, Z., Liu, M., and Yin, M.: Thermokarst lake changes between 1969 and 2010 in the Beilu River Basin, Qinghai-Tibet Plateau, Chinese Sci. Bull., 60(5), 556-564, 2015.

Mironov, D., Terzhevik, A., Kirillin, G., Jonas, T., Malm, J. and Farmer, D.: Radiatively driven convection in ice-covered lakes: Observations, scaling, and a mixed layer model, J. Geophys. Res., 107(C4), 3032, doi: 10.1029/2001JC000982, 2002.

Mountain Research Initiative EDW Working Group: Elevation-dependent warming in mountain regions of the world, Nature Clim. Change, 5, 424-430, 2015.

Niu, F., Lin, Z., Liu, H., and Lu, J.: Characteristics of thermokarst lakes and their influence on permafrost in Qinghai-Tibet Plateau, Geomorphology, 132, 222-233, 2011.

Nordbo, A., Launiainen, S., Mammarella, I., Leppäranta, M., Houtari, J., Ojala, A., and Vesala, T.: Long-term energy flux measurements and energy balance over a small boreal lake using eddy covariance technique, J. Geophys. Res., 116, D02119, doi: 10.1029/2010JD014542, 2011.

Pan, X., Yu, Q., and You, Y.: Role of rainwater induced subsurface flow in water-level dynamics and thermoerosion of shallow thermokarst ponds on the Northeastern Qinghai-Tibet Plateau, The Cryosphere Discuss., 8, 6117-6146, 2014.

Rizk, W., Kirillin, G., and Leppäranta, M.: Basin-scale circulation and heat fluxes in ice-covered lakes, Limnol. Oceanogr., 59(2), 445-464, , 2014.

Semmler, T., Cheng, B., Yang, Y., and Rontu, L.: Snow and ice on Bear Lake (Alaska)-sensitivity experiments with two lake ice models, Tellus A, 64, 17339, doi:10.3402/tellusa.v64i0.17339, 2012.

Shi, L., Li, Z., Niu, F., Huang, W., Lu, P., Feng, E., and Han, H.: Thermal diffusivity of thermokarst lake ice in the Beiluhe basin of the Qinghai-Tibet Plateau, Ann. Glaciol., 55(66), 153-158, 2014.

Su, F., Zhang, L., Ou, T., Chen, D., Yao, T., Tong, K., and Qi, Y.: Hydrological response to future climate changes for the major upstream river basins in the Tibetan Plateau, Global Planet. Change, 136, 82-95, 2016.

Tian, B., Li, Z., Engram, M. J., Niu, F., Tang, P., Zou, P., and Xu, J.: Characterizing C-band backscattering from thermokarst lake ice on the Qinghai-Tibet Plateau, ISPRS J. Photogramm. Remote Sens., 104, 63-76, 2015.

Vesala, T., Houtari, J., Rannik, U., Suni, T., Smolander, S., Sogachev, A., Launiainen, S., and Ojala, A.: Eddy covariance measurements of carbon exchange and latent and sensible heat fluxes over a boreal lake for a full open-water period, J. Geophys. Res., 111, D11101, doi: 10.1029/2005JD006365, 2006.

Wang, B., Ma, Y., Chen, X., Ma, W., Su, Z., and Menenti, M.: Observation and simulation of lake-air heat and water transfer processes in a high-altitude shallow lake on the Tibetan Plateau, J. Geophys. Res., 120, 12327-12344, 2015.

Wen, L., Lyu, S., Kirillin, G., Li, Z., and Zhao, L.: Air-lake boundary layer and performance of a simple lake parameterization scheme over the Tibetan highlands, Tellus A, 68, 31091, doi:10.3402/tellusa.v68.31091, 2016.

Wen, L., Lyu, S., Li, Z., Zhao, L., and Nagabhatla, N.: Impacts of the two biggest lakes on local temperature and precipitation in the Yellow River Source Region of the Tibetan Plateau, Adv. Meteorol., 2015, 248031, doi:10.1155/2015/248031, 2015.

Wright, D.M., Posselt, D.J., and Steiner, A.L.: Sensitivity of lake-effect snowfall to lake ice cover and temperature in the Great Lakes region, Mon. Weather Rev., 141, 670-689, 2013.

Wu, G., Duan, A., Liu, Y., Mao, J., Ren, R., Bao, Q., He, B., Liu, B., and Hu, W.: Tibetan Plateau climate dynamics: recent research progress and outlook, Natl. Sci. Rev., 2, 100-116, , 2015.

Wu, Q., Zhang, P., Jiang, G., Yang, Y., Deng, Y., and Wang, X.: Bubble emissions from thermokarst lakes in the Qinghai-Xizang Plateau, Quatern. Int., 321, 65-70, 2014.

Yang, K., Ye, B., Zhou, D., Foken, T., Qin, J., and Zhou, Z.: Response of hydrological cycle to recent climate changes in Tibetan Plateau, Climatic Change, 109, 517-534, 2011.

Yang, X., Lyu, Y., Ma, Y., and Wen, J.: Summertime thermally-induced circulations over the Lake Nam Co region of the Tibetan Plateau, J. Meteorol. Res., 29(2), 305-314, 2015.

Yang, Y., Leppäranta, M., Cheng, B., Heil, P., Li, Z.: Numerical modeling of snow and ice thickness in Lake Vanajävesi, Finland, Tellus A, 64, 17202, doi:10.3402/tellusa.v64i0.17202, 2012.

Zhang. G., Yao, T., Xie, H., Zhang, K., and Zhu, F.: Lakes' state and abundance across the Tibetan Plateau, Chinese Sci. Bull., 59(24), 3010-3021, 2014.

Hydrol. Earth Syst. Sci. Discuss., https://doi.org/10.5194/hess-2018-616
Manuscript under review for journal Hydrol. Earth Syst. Sci.
Discussion started: 21 December 2018

Hydrology and Earth System Sciences Discussions
Open Access

Table 1. Parameters and input data applied in the model reference run

Variables	Value	Source
V_a, T_a, Rh, Q_s, Q_l	Time series	Observations at BWS
Ice density ρ_i	900 kg m^{-3}	Huang et al. (2012, 2013)
Thermal conductivity k_i	1.80 W m^{-1} K^{-1}	Huang et al. (2013)
Albedo α	0.1- 0.55	Briegleb et al. (2004)
Ice extinction coefficient κ_i	(1.5–17) m^{-1}	Launiainen and Cheng (1998) adapted from Grenfell and Maykut (1977)
Bottom heat flux F_w	Time series	Parameterized based on in-ice temperature profile and ice bottom growth rate (Huang et al., to be submitted)
Initial ice thickness	0.05 m	Observation
Initial ice temperature	Linear interpolation between T_a and T_b	Calculation

Table 2. The mean bias error (*MBE*), mean absolute error (*MAE*), standard deviation (*STD*), root mean square error (*RMSE*), and correlation coefficient (*R*) between modeled and observed ice mass balance components with *n*=4023 (in cm)

Items	Surface	Bottom	Total mass balance
MBE	0.2	4.2	4.1
MAE	2.5	4.8	4.3
STD	2.9	3.6	3.0
RMSE	2.9	5.5	5.0
R	0.97	0.99	0.99

Table 3. The monthly means of heat fluxes (in W m^{-2}) within the air-ice-water column. Q_s: incident solar radiation; Q_{sn}: net solar radiation; Q_{ss}: net solar radiation for surface heat balance; Q_{ln}: net longwave radiation; Q_h: sensible heat flux; Q_{le}: latent heat flux; F_c: surface conductive heat flux; F_m: net surface heat flux, that is, the sum of Q_{ss}, Q_{ln}, Q_h, Q_{le} and F_c; Q_{si}: solar radiation absorption within the ice interior; Q_{sw}: solar radiation into under-ice water; F_w: heat flux from water into ice.

Month	11	12	1	2	3	4
Q_s	162	142	138	176	208	259
Q_{sn}	110	69	63	110	135	169
Q_{ss}	37	30	32	57	65	62
Q_{ln}	-112	-100	-83	-87	-79	-73
Q_h	-10	15	15	17	-1	4
Q_{le}	-46	-31	-32	-54	-53	-53
F_c	125	85	68	68	69	63
F_m	-6	-0.1	0.1	0.2	2	4
Q_{si}	35	26	23	40	49	63
Q_{sw}	39	14	8	14	21	43
F_w	34	21	20	20	21	36

Hydrol. Earth Syst. Sci. Discuss., https://doi.org/10.5194/hess-2018-616
Manuscript under review for journal Hydrol. Earth Syst. Sci.
Discussion started: 21 December 2018

Hydrology and Earth System Sciences
Open Access
Discussions

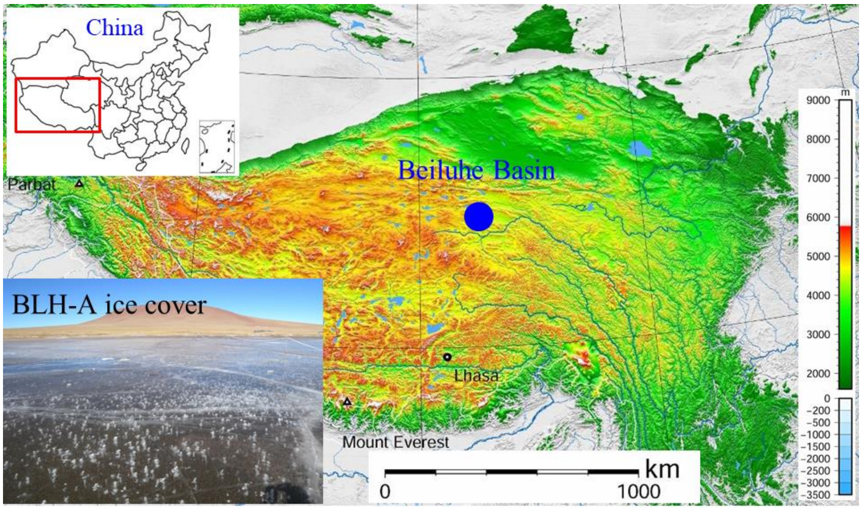

Figure 1. General view of QTP and location of the study area

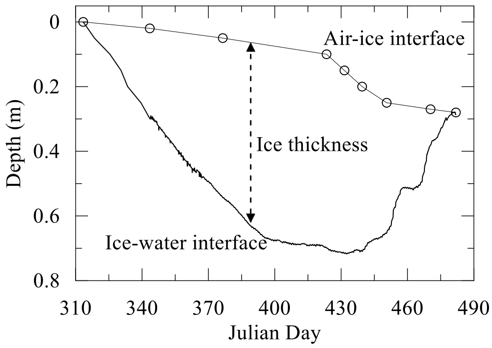

Figure 2. The observed lake ice thickness evolution over the whole 2010/2011 ice season. The open circles denote the observed location of the ice surface, and the solid lines connecting the circles denote the linear interpolation.

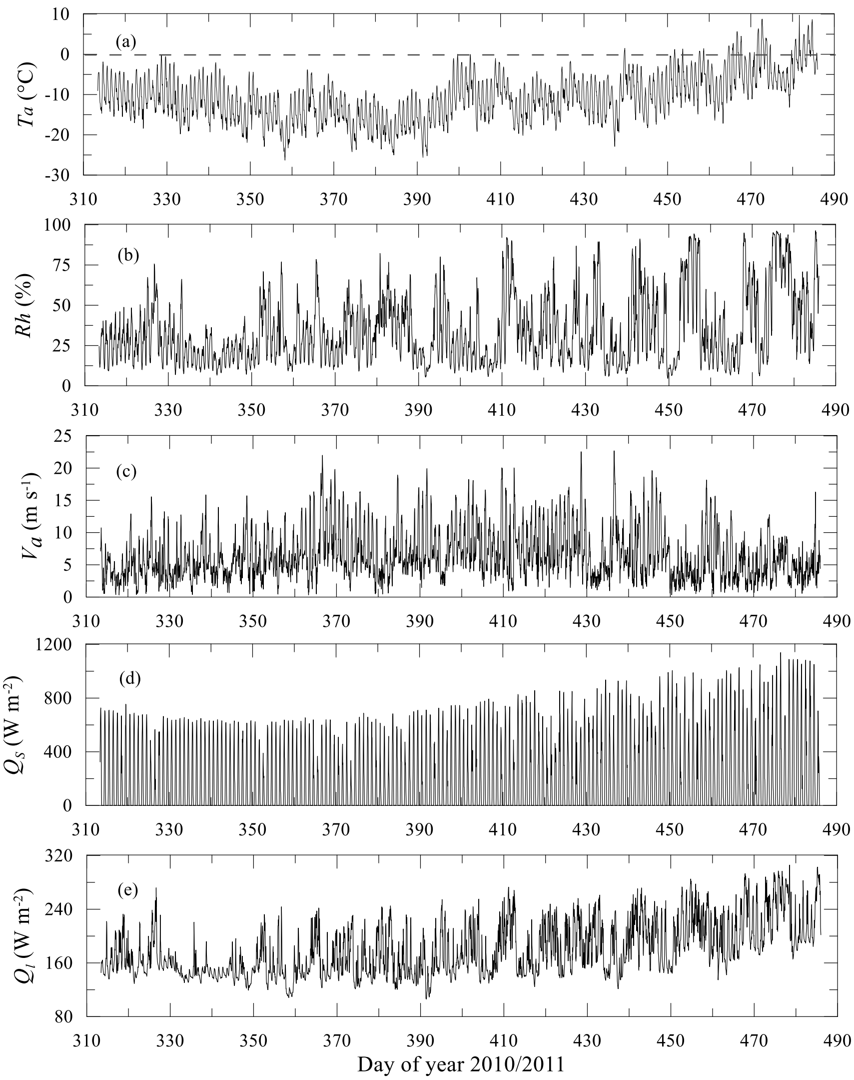

Figure 3. The time series of observed meteorological variables through the whole ice season of 2010-2011. (a) daily mean air temperature T_a, (b) relative humidity Rh, (c) wind speed V_a, (d) incident shortwave solar radiation Q_s, and (e) incident longwave radiation Q_l.

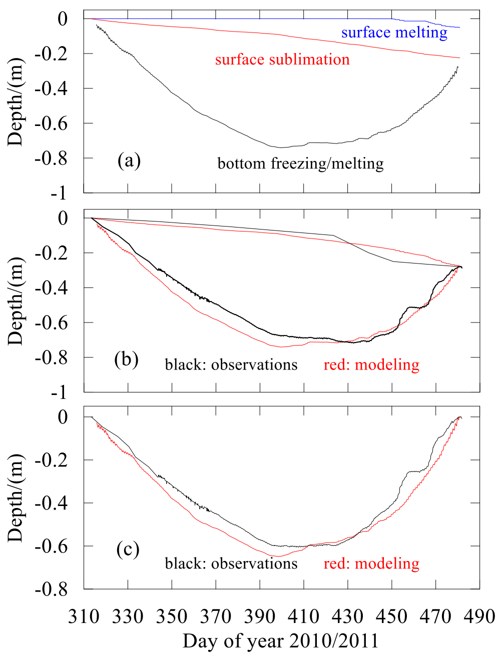

Figure 4. The HIGHTSI modeled BLH lake ice mass balance components (a), the ice surface and bottom evolution (b), and the ice thickness (c).

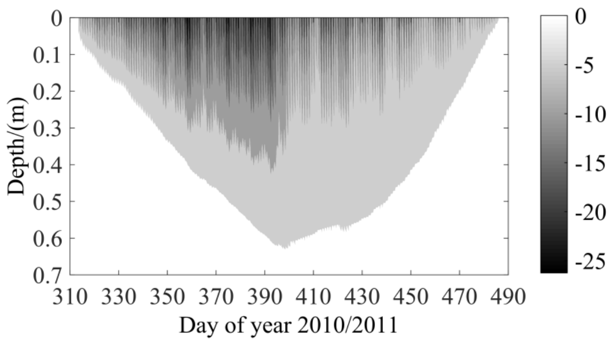

Figure 5. HIGHTSI modeled ice temperature regime for winter 2010/2011.

Hydrology and Earth System Sciences
Open Access
Discussions

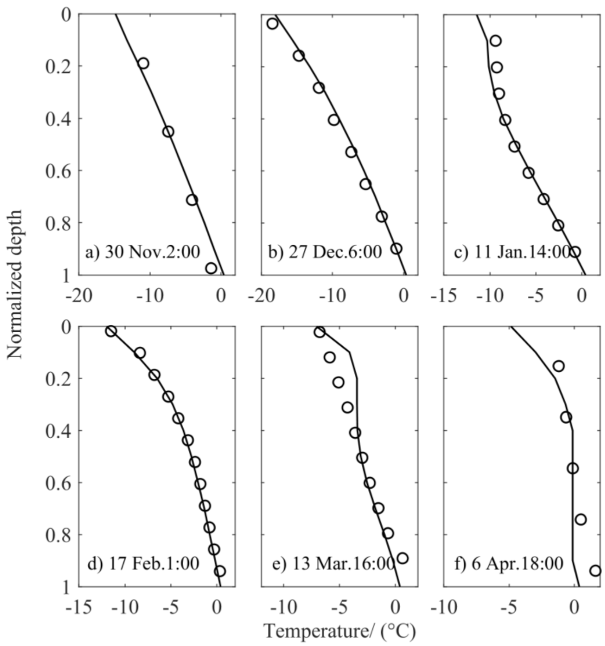

Figure 6. Comparisons of modeled (lines) and observed (circles) vertical temperature profiles of within ice at selected time steps. A normalized depth (depth divided by ice thickness) is used as the y-axis (0 and 1 denote the ice surface and bottom, respectively).

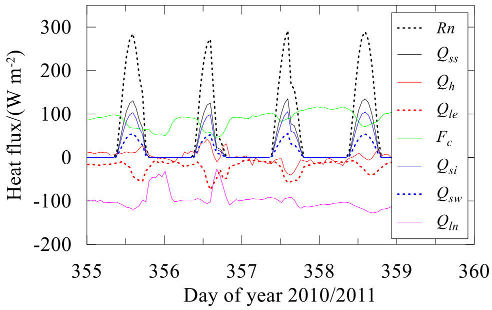

Figure 7. Diurnal patterns of various radiation/heat fluxes

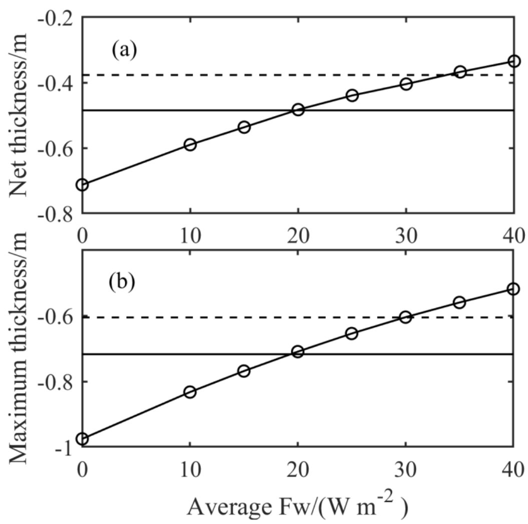

Figure 8. Modeled (lines with circles) average (a) and maximum (b) ice thickness applying different constant F_w. The broken lines are observed average and maximum ice thickness during the simulation period. The solid lines are observed average and maximum ice growth at ice bottom.

Hydrol. Earth Syst. Sci. Discuss., https://doi.org/10.5194/hess-2018-616
Manuscript under review for journal Hydrol. Earth Syst. Sci.
Discussion started: 21 December 2018

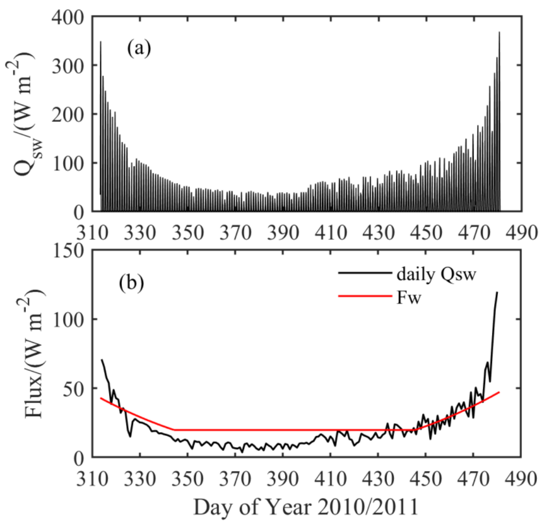

Figure 9. Modeled solar radiation penetration (Q_{sw}) into the under-ice water column: hourly (a) and daily averages (b) with prescribed F_w during the simulation period.

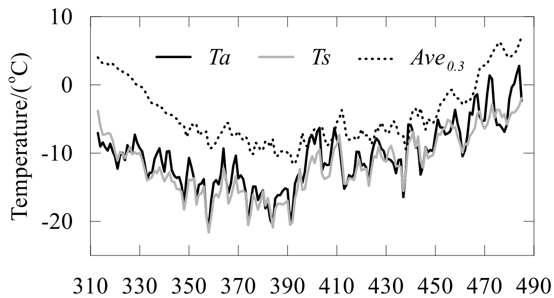

Figure 10. Daily means of the observed air temperature (T_a), the averaged ice/water temperature of the top 30 cm ($Ave_{0\text{-}0.3}$), and the calculated ice surface temperature (T_s).

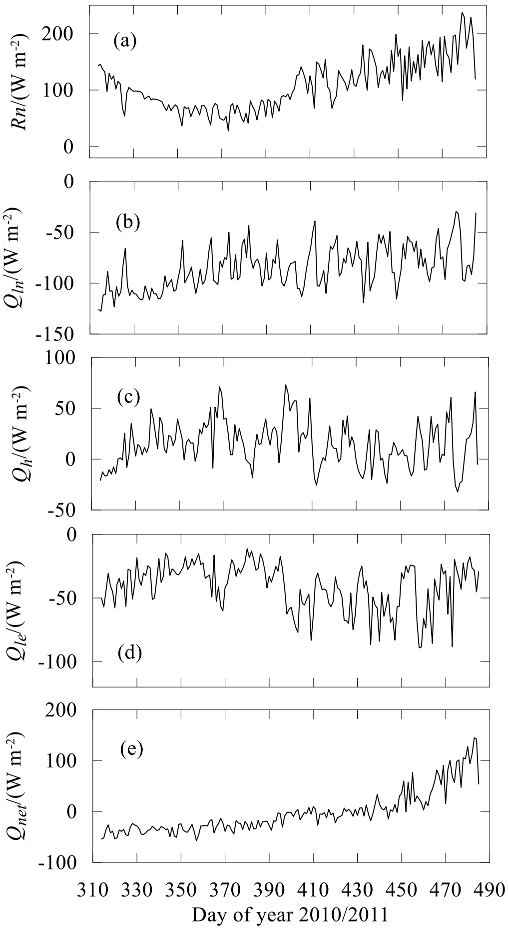

Figure 11. Daily means of the surface energy balance components of net shortwave (Q_{sn}) and longwave (Q_{ln}) radiation, turbulent sensible (Q_h) and latent (Q_e) heat fluxes, and net flux into the lake (Q_{net}= Q_{sn}+Q_{ln}+Q_h+Q_{le}) though the entire ice season.

Hydrol. Earth Syst. Sci. Discuss., https://doi.org/10.5194/hess-2018-616
Manuscript under review for journal Hydrol. Earth Syst. Sci.
Discussion started: 21 December 2018

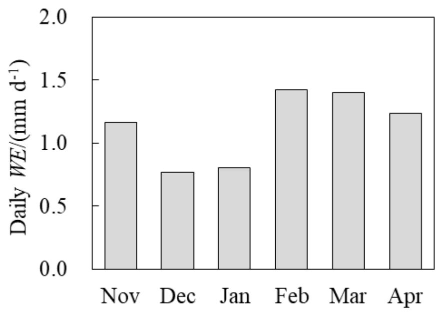

Figure 12. The daily mean surface sublimated water equivalent through the winter 2010/2011.